Flow Characteristics of a Mixed Compression Hypersonic Intake

J. K. James[†] and H. D. Kim

Department of Mechanical Engineering, Andong National University, Andong,36729, Republic of Korea

†*Corresponding Author Email: jintu@pyunji.andong.ac.kr*

ABSTRACT

The flow field in a two-dimensional hypersonic mixed-compression inlet in a freestream Mach numbers of M_∞ =2.0, 3.0, and 5.0 are numerically solved to understand the effect of throat area variation. The exit area ratio variation is simulated by placing a plug insert at different axial locations at the exit of the model. The flow field is achieved computationally by solving the Reynolds Averaged Navier-Stokes equations in a finite volume framework. For each flow condition, the variation in shock structure is analyzed and the variation of the oblique shock wave angle with the mass flow rate is calculated theoretically and compared with the present CFD analysis. The variation in oblique shock angle is calculated in terms of the mass flow rate by considering the capture area and spillage flow through the inlet. The theoretical results suggest that the method can predict the inlet operating conditions at different freestream Mach numbers and area ratios. This method can quantify the reduction in mass flow rate due to the throttling effect by analyzing the flow field shock pattern. The effects of various important performance parameters such as free stream Mach number, total pressure recovery, and mass flow ratio were then numerically investigated. As the Mach number is increased, the total pressure recovery is reduced, but the maximum value of the mass flow rate is increased. The analysis is also focused on the effect of throat area variation on performance parameters at each Mach number. The characteristic curve of the inlet is then obtained for each free stream Mach number.

Keywords: Supersonic intake; Flow separation; Performance parameters; Shock wave angle, Supersonic flow.

NOMENCLATURE

A	cross-sectional area		SWBLI	Shock Wave Boundary Layer Interaction
C	cowl lip point			
d	maximum diameter of the inlet model		TPR	Total Pressure Recovery
h	stream tube height		x, y, z	Cartesian coordinates
H_c	captured stream tube height at design condition		$\dot{m}$	mass flow rate
			ψ	area ratio of throat
L	length of the inlet model		θ	semi-cone angle
M	Mach number		β	shock angle
p	static pressure		ζ	ratio of captured to the theoretical mass flow rate
P_0	stagnation pressure			

1. INTRODUCTION

The performance of a hypersonic propulsion system is greatly affected by the flow characteristics through the intake. The main objective of an intake in this system is to decelerate the incoming flow to a relatively low velocity with minimum possible losses while maintaining maximum possible uniform flow (Curran and Murthy 2001; Marguart 1991; Raj and Venkatasubbaiah 2012). In general, hypersonic vehicles operate at very high altitudes yielding a higher service ceiling encounter with very low air pressure and density (Fan 2011). The required pressure rise at a very high altitude is achieved by mixed compression inlets (Van Wie *et al.* 1996) where the required compression is achieved by the external compression from the compression ramp and through a system of multiple shocks inside the

duct (Weir *et al.* 1989). In a supersonic inlet, there are various flow phenomena such as shock waves and their interaction, internal and external shocks, and boundary layer separation. This makes the flow field of an inlet complex and the analysis becomes difficult. Many studies have been conducted to measure or calculate the performance parameters of the inlet using experimental and numerical tools. Inside the inlet duct or isolator, there can be the formation of multiple shock wave reflections and this further compresses the flow before being fed to the combustion chamber (Li *et al.* 2017, 2018; Ram *et al.* 2020; Wang *et al.* 2020). The internal flow field encounters the shock wave boundary layer interaction (SWBLI) and this makes the flow field unsteady (Clemens and Narayanaswamy 2014). The main aims of these studies were to find out the characteristics of the flow field around and inside an inlet as well as the effects of free-stream conditions on the inlet performance.

The intake performance can be evaluated by considering different variables such as total pressure recovery, mass flow ratio, and flow distortion. The effects of cowl deflection angle, bleed, and back pressure on the performance parameters was carried out (Das and Prasad 2009, 2010) for mixed compression intake. While other studies considered the effect of free-stream Mach number along with other flow parameters to understand the intake performance in detail (Gokhale and Kumar 2001; Soltani *et al.* 2013). In most of the previous studies, the variation in Mach number is achieved by varying the static pressure ahead of the inlet with a constant stagnation pressure. But several situations would occur that the hypersonic propulsion system needs to accelerate and decelerate at a constant altitude. During such operations, the static pressure remains constant and the corresponding stagnation pressure varies to accommodate the Mach number variation. In the present study also, the stagnation pressure is varied to reflect this Mach number variation by considering that the propulsion system is operating at a constant altitude.

There are various numerical methods to simulate the flow and to predict the performance parameters. Computational fluid dynamics (CFD) approaches along with optimization techniques are employed to predict the performance of an inlet. The earlier studies conducted parametric studies by varying the major geometrical parameters such as cone angle or cowl leading-edge radius to get the desirable performance (Chen *et al.* 2005a, b; Zha *et al.* 1997). Hypersonic inlets have also been analyzed in the recent past (Chang *et al.* 2009; Liang *et al.* 2008; Nair *et al.* 2005; Xiang *et al.* 2020a) The analysis of 3D inlets with sidewall compression (Xiang *et al.* 2020b) and the investigation of 3D shock interactions over wedges (Xiang *et al.* 2021; Xiang *et al.* 2016) provided a detailed study on the shock interaction problems in the intake flow field. A detailed aerodynamic analysis was conducted by Nair et al. (Nair *et al.* 2005) using Reynolds-averaged Navier–Stokes to compute the flow through a hypersonic inlet. The effects of the position of the sidewall compression and the cowl deflection

angle on the inlet performance were computed to improve the mass flow rate at the design point. The studies were extended to other Mach numbers of 4 and 6. The results showed that the sidewall compression affects the mass flow, whereas the cowl deflection angle manipulates the inlet starting characteristics.

The shock system associated with the inlet flow is highly susceptible to the fluctuations in the combustion chamber or the inlet backpressure. The inlet shock pattern for a mixed compression inlet operating at supercritical conditions is depicted in Fig.1. The incoming supersonic flow generates an oblique shock wave from the apex of the center body and the other oblique shock wave generated from the cowl lip is reflected inside the duct. Thus, the required compression is achieved partially through external compression and remaining internally through multiple shock reflections before being fed to the combustion chamber. The inlet can operate at different conditions depending on the incoming flow conditions or the downstream disturbances caused by combustion instability. In supersonic inlets, the buzz is an unsteady phenomenon that is self-sustained occurs when the intake operates in the subcritical condition. During this phase of operation, the shock wave oscillates along the inlet and causes mass flow fluctuations inside the engine and it can lead to combustion instability, engine surge, and/or thrust loss, which results in deterioration of the performance of the propulsion system (K James *et al.* 2021). A series of wavefronts push the flow outside the intake to accommodate the appropriate mass flow for the downstream conditions. To accommodate the mass flow change, the oblique shock wave changes its angle and feeds a reduced mass flow to the inlet. During that process, the steady flow is instantaneously breaking down and a new steady state is initiated. The reduction in mass flow rate through the inlet is related to the oblique shock wave angle and this phenomenon is not very much studied earlier.
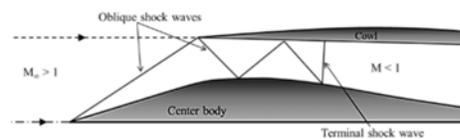

Fig. 1. Inlet shock pattern of mixed compression inlet at the supercritical condition

Even though there are many attempts to predict and improve the flow characteristics around and inside the inlets to obtain the performance parameters, but the predictions are not still reliable. Each inlet has its special characteristics that could not be accurately predicted yet. Besides, the relation between the oblique shock angle and the mass flow rate through the inlet is not studied in detail. Therefore, in the present study, an axisymmetric mixed compression inlet designed to operate at a freestream Mach number of 2.0 is analyzed for a range of free-stream
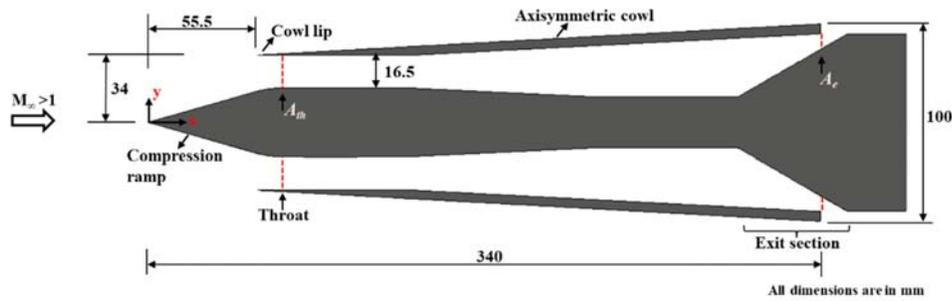
Fig. 1. Schematic of the supersonic intake model.

Mach numbers. The variation of different performance parameters at different Mach numbers and different area ratios is performed computationally. The present study also aims to analytically predict the relation between the oblique shock wave angle and the mass flow rate through the inlet.

2. NUMERICAL METHODOLOGY

2.1 Problem description

An axisymmetric mixed compression inlet model, as shown in Fig.2 is considered to study the performance parameters. A generic hypersonic flight Mach number of $M\infty = 2.0$ is taken as the operational reference at sea level conditions. The total length and the maximum diameter of the inlet are L=340mm and d=100mm. the semi-cone angle of the center body is 16 degrees and the intake system are kept at an angle of attack of zero degrees to the incoming flow. At the design operating condition, the oblique shock wave is on the cowl lip and makes the external part of the compression process. Further compression is achieved inside the isolator part of the inlet system which is 0.18 times the total length of the inlet. The rest of the current inlet's geometrical features are adopted from the experimental work by Abedi et al (Abedi *et al.* 2020).

For each free stream Mach number, the exit throat area was changed by moving the plug (wedge) to study the effect of mass flow rate variation on the inlet performance as shown in Fig.2. The area ratio of the throat (ψ = Ae/Ath) is defined as the ratio of flow area at the exit plane to the throat area of the inlet model. Therefore, ψ = 0.0% means that the exit area of the inlet is completely closed in the present arrangement.

2.2 Computational domain and meshing

Figure 3 shows the computational domain and the axisymmetric grid system of the inlet along with the boundary conditions. The inlet is placed in a freestream condition and it is achieved by providing far-field boundary conditions as shown in Fig. 3(a). The pressure outlet boundary condition is given at the end of the computational domain. All other edges forming the cowl and ramp surfaces are treated as non-adiabatic and no-slip boundaries except the axis

line. The apex of the ramp surface is taken as the origin and all the measurements were taken based on this point. Figures 3(b) and (c) indicate the enlarged view of the computational domain at some critical locations and it also shows the growth of the boundary layer grid provided. A compact domain and an appropriate meshing strategy reduce the overall mesh counts and save the computational time required to resolve the flow. The fluid dynamics inside the inlet are of primary importance in the present study. A structured meshing scheme is adopted, and the turbulence wall parameter (y+) is kept less than one to resolve the boundary layer effects. The progression of mesh cell spacing in the isolator is not kept more than1.15. Numerical analysis is performed using a commercial computational fluid dynamics (CFD) package from Ansys-Fluent®. The solver discretizes the fluid domain based on the finite volume schemes. The fluid turbulence is modeled using a shear stress transport (Menter 1993; Menter 1994) based two-equation eddy viscosity model called SST-kω which is known to predict the hypersonic inlet flow features as seen in the experiments (Lee and Kang 2019; Roy and Blottner 2006; Wang and Guo 2013).

The validation of the chosen turbulence model with experiments in hypersonic inlet flow is discussed in the following section. The flow field is solved with air as the ideal gas, and the fluid's viscosity is computed through Sutherland's three equation model. All the flow equations are discretized spatially (implicit) with second-order accuracy. The AUSM flux type was taken and the gradients are resolved using Lease Squares Cell-based techniques.

Two-dimensional structured meshes are generated at different mesh densities as indicated in Fig. 4 to find the dependence of mesh density on the final numerical solution and also to validate the adopted solver. Experiments of Abedi et al. (Abedi *et al.* 2020) are considered for the mesh independence and solver validation exercises. The variation of the mass flow rate through the inlet system is depicted in Fig. 4. It shows that the mesh with ($2x10^5$) cells would be sufficient to obtain steady-state results. For quantitative comparisons, experimental wall-static pressure measurements ($p/P_{0\infty}$) obtained on the ramp surface of the intake are compared with the numerical results as shown in Fig. 5. The freestream stagnation pressure is used to non-dimensionalize the
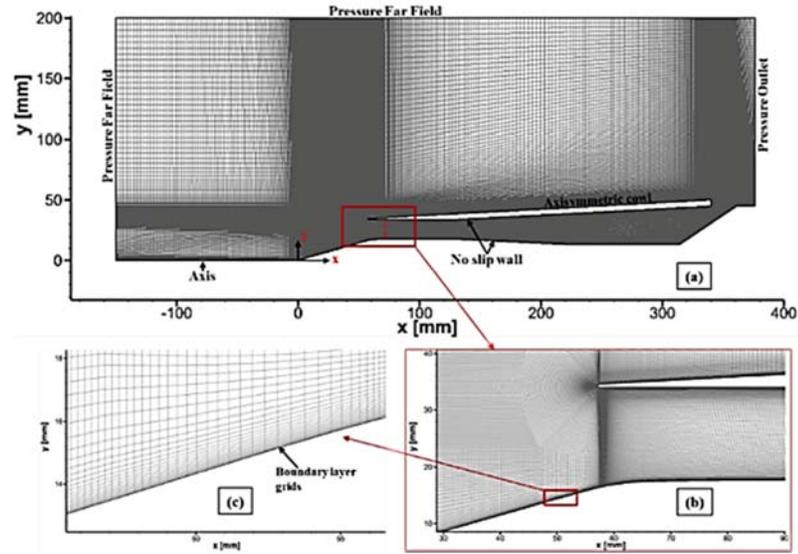
Fig. 3. (a) Grid system in the computational domain with the boundary conditions. (b) and (c) Enlarged view of the computational grids.
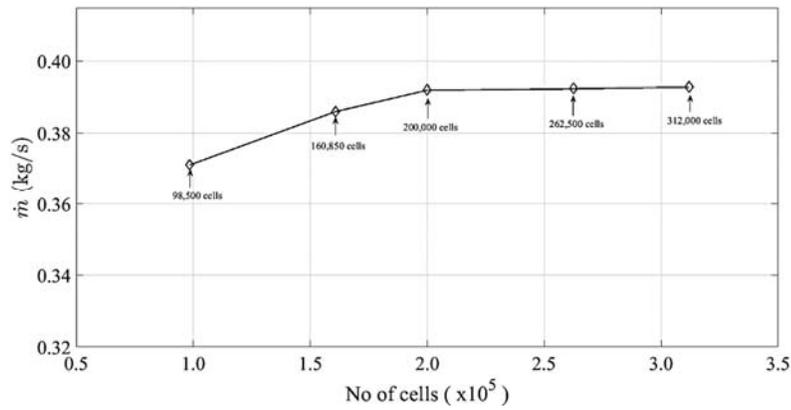

Fig. 2. Variation of the mass flow rate through the intake for different mesh sizes.
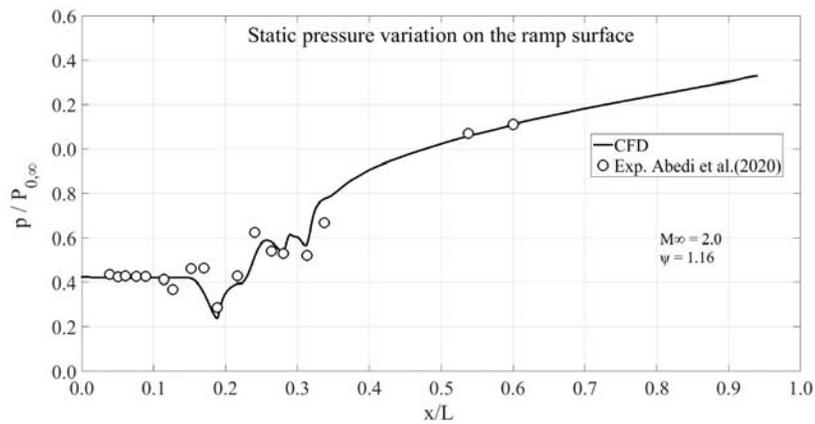

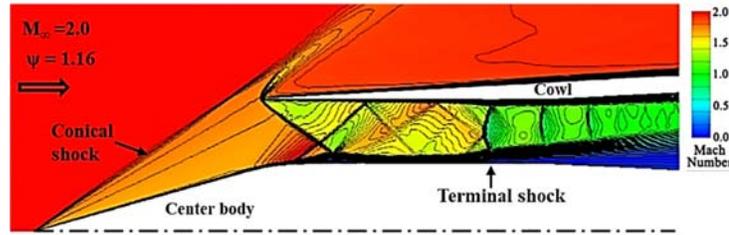**Fig. 3. Variation of static pressure along the ramp surface for a Mach number of 2.0 and area ratio of 1.16.**

Fig. 4. Contours of Mach number for the case with an inlet Mach number of 2.0 and ψ =1.16, showing the shock structure associated with the flow field.
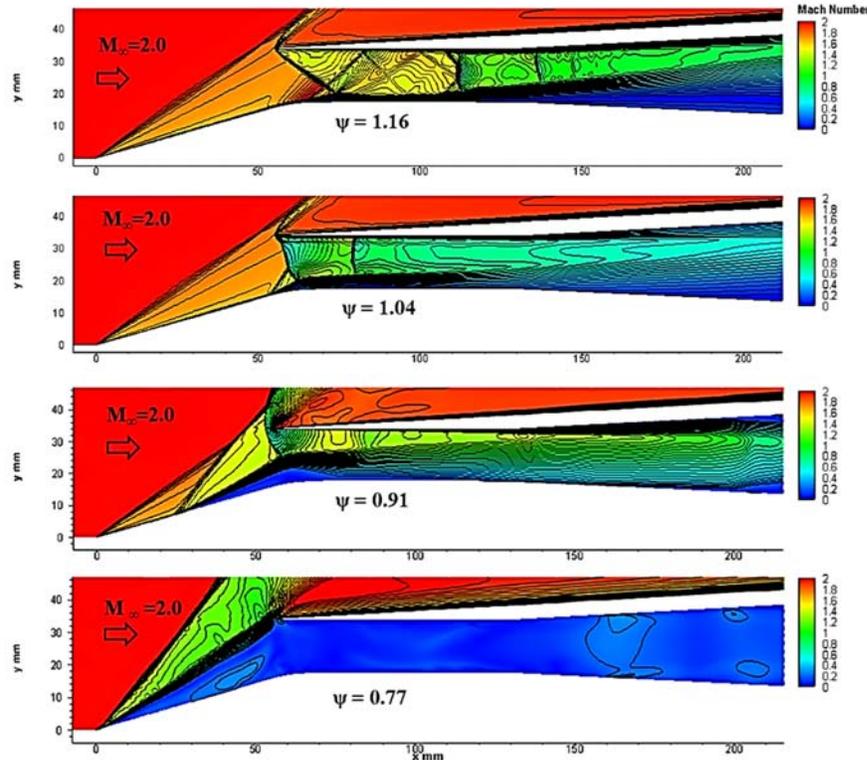

Fig. 5. Variation of Mach contours at different area ratio for an inlet Mach number of 2.0. The changes in shock patterns are illustrated in this figure.

state solution for different Mach numbers and different area ratios are studied in this work. The performance parameters such as the total pressure recovery, mass flow rate, etc. are analyzed along with the oblique shock wave angle variation.

3. RESULTS AND DISCUSSION

3.1 Analysis of shock structure at different Mach number and area ratio

The inlet performance at several free stream Mach numbers and different area ratios (ψ) are discussed in this section. Furthermore, the characteristic curves of the inlet for all Mach numbers are calculated and examined. Figure 6 shows the Mach contour to indicate the shock structure in the flow field at a free-stream Mach number of 2.0 and an area ratio of 1.16.

It is observed that the conical shock is formed from the apex of the center body and allowed to impinge on the cowl lip. The isolator's steady flow field consists of reflecting shocks between the cowl and ramp wall of the isolator. Firstly, the cowl shock impinges on the ramp wall's shoulder and results in the flow separation due to the shock-wave boundary layer interaction (SWBLI) and leads to the formation of a separation bubble of considerable thickness. The induced separation shock from the separation bubble further hits the cowl wall reflects the ramp surface. The eventual interactions end at the terminal shock and which can be considered as the first shock in the shock train system.

The flow features are extracted and presented for different area ratios at a free-stream Mach number of 2.0 as shown in Fig. 7. It is observed that as the area ratio is increased, the shock system is pushed
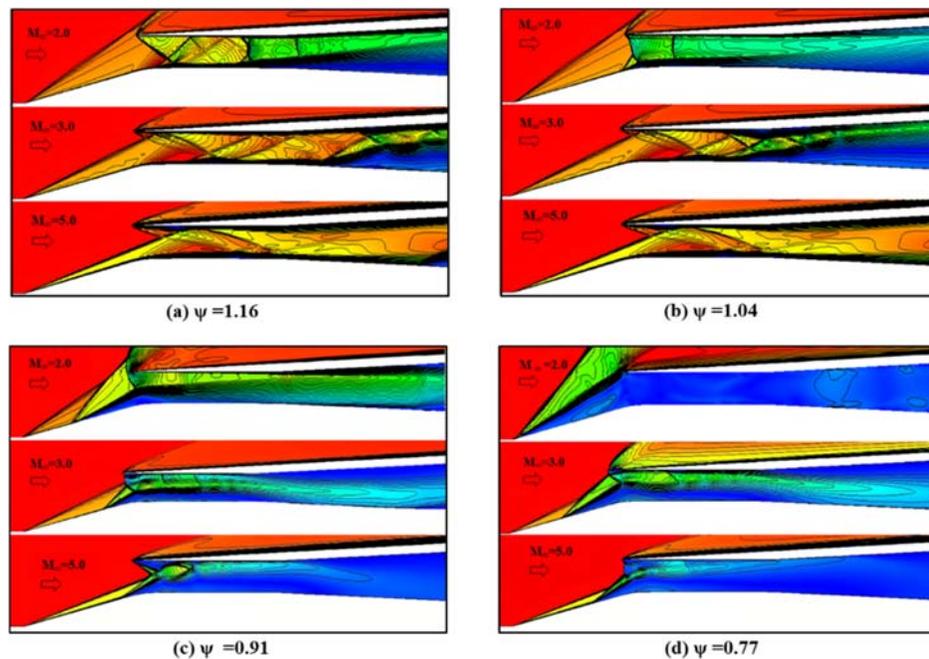
Fig. 6. Variation of Mach contours at different area ratios for an inlet Mach number of 2.0, 3.0, and 5.0.

upwards. At $\psi=1.16$, the intake is started or in other words, it is said to be operating at supercritical conditions. As ψ is reduced to $\psi=1.04$ by moving the downstream plug inside, the shock deviates from its supercritical condition. The terminal shock is pushed upstream and is located slightly upstream of the cowl lip. It is also noted that at this ψ value, the shock on the ramp surface forms a λ-shock, and the SWBLI makes a relatively larger flow separation in the ramp surface. The size of the separation region grows big as the flow proceeds downstream. The separation region reduces the available flow area through the intake in the cowl lip region and the re-acceleration of the flow occurs. This creates another shock wave downstream of the terminal shock. The subsonic flow is then fed to the combustion chamber. Upon increasing the area ratio to $\psi=0.91$, the shock system completely expels out of the cowl lip region. Another oblique shock wave is formed on the compression ramp and this deviates the oblique shock angle in the vicinity of the cowl lip region. A large separation is formed at the foot of the second oblique shock wave and a bow shock wave is formed near the cowl lip region. Since the oblique shock wave angle is changed, this implies a reduced mass flow rate through the inlet. In this condition, the inlet operates in subcritical conditions. When we reduce the area ratio further to 0.77, the shock system moves upstream and reaches the ramp apex point. During this phase of operation, a completely subsonic flow is entering the inlet and the oblique shock angle is at its maximum value producing the lowest mass flow rate through the inlet. The supersonic flow after the oblique shock spills over the cowl lip.

The effect of area variation and Mach number variation in terms of shock structure is shown in Fig. 8. As the Mach number is increased, the oblique shock wave angle from the ramp apex is reduced.

Figure 8(a) indicates the variation in Mach contour at different freestream Mach numbers for $\psi=1.16$. At this value of area ratio, the inlet operates in supercritical conditions. As the Mach number is increased, the oblique shock impinges at a downstream location on the cowl inner surface. The reflected shock angle is relatively small and hence the boundary layer separation is also reduced. When $\psi=1.04$, the flow corresponding to M=2 is operating at subcritical condition, while M=3 and M=5 are at supercritical operating mode. The inlet changes to the subcritical mode for M=2 and M=3 when $\psi=0.91$. The inlet is operating at subcritical mode (Fig. 8(d)) for all the Mach numbers when $\psi=0.77$. Another two area ratio values of $\psi=1.10$ and $\psi=0.97$ are computed to obtain more details on the performance parameter and are discussed in the following section.

3.2 Relationship between mass flow rate and the shock angle

The schematic of the hypersonic inlet flow field and the shock structure is shown in Fig. 9. The center body has a semi cone angle of θ is encountering a flow with freestream Mach number of M_∞. The inlet cowl lip makes a radius of H_c and at design condition, the oblique shock wave is impinging on the cowl lip with an angle of $\beta1$. The theoretical maximum capture area of flow is decided by the parameter H_c. The streamline at H_c height impinges on the cowl lip
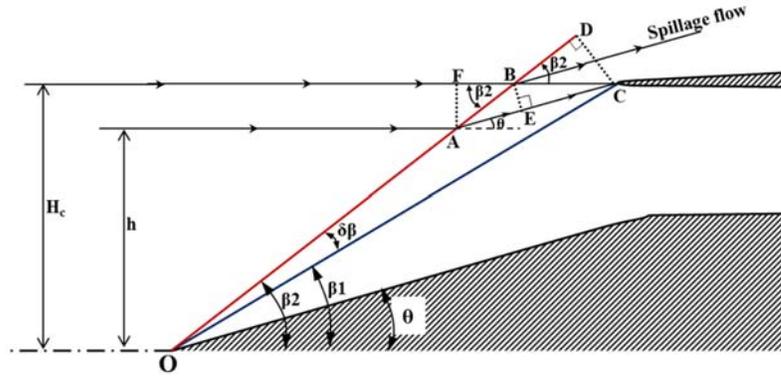
Fig. 7. Schematic of the flow field and shock pattern in an inlet model.

at the supercritical operating condition. It is assumed that during the inlet operation, the oblique shock wave has changed the angle to a new value of β2, which is larger than the design value. This makes some part of the flow to be spilled over the cowl lip and hence reduces the mass flow rate through the inlet. The new limiting streamlines at a height of 'h' will now impinge on the cowl lip at a shock angle of β2. This scenario is depicted in Fig. 9 by considering that the change in the oblique shock angle is small. The mass flow calculated by considering the distance between H_c and h is termed as the spillage flow.

The limiting streamline at new oblique shock wave angle β2 intersects at cowl lip point C (after passing through the point A), reducing the incoming flow area from Hc to h. The new flow area can be calculated based on the schematic as,

$$h = H_c - AF \tag{1}$$

From triangles AFB and AEB,

$$AF = AB * \sin \beta_2 \tag{2}$$

and

$$AB = \frac{BE}{\sin(\beta_2 - \theta)} \tag{3}$$

Similarly, on solving the geometrical parameters, it reduces to

$$AF = \frac{OC * \tan(\beta_2 - \beta_1) * \sin \theta}{\sin(\beta_2 - \theta)} \tag{4}$$

From the geometry we also have

$$OC = \frac{H_c}{\sin(\beta_1)} \tag{5}$$

Therefore Eq. 4 will be

$$AF = H_c * \frac{\tan(\beta_2 - \beta_1) * \sin \theta}{\sin(\beta_1) * \sin(\beta_2 - \theta)} \tag{6}$$

Using the above Eq. 6 into Eq. 1, we get

$$h = H_c \left\{ 1 - \frac{\tan(\beta_2 - \beta_1) * \sin \theta}{\sin(\beta_1) * \sin(\beta_2 - \theta)} \right\} \tag{7}$$

or

$$h = H_c \{1 - k\} \tag{8}$$

For the 2D planar inlet model,

The undisturbed maximum mass flow rate is,

$$\dot{m}_{\text{theory}} = H_c * \frac{p_\infty M_\infty \sqrt{\gamma}}{\sqrt{(RT_\infty)}} \tag{9}$$

And the disturbed/captured mass flow at larger β2 is

$$\dot{m}_{cap} = h * \frac{p_\infty M_\infty \sqrt{\gamma}}{\sqrt{(RT_\infty)}} \tag{10}$$

The mass flow ratio, MFR,

$$\dot{m}_{cap}/\dot{m}_{\text{theory}} = h/ H_c \tag{11}$$

Therefore,

$$\xi = \dot{m}_{cap}/\dot{m}_{\text{theory}} = 1 - k \tag{12}$$

For an axisymmetric inlet model,

$$\xi = \dot{m}_{cap}/\dot{m}_{\text{theory}} = (1 - k)^2 \tag{13}$$

The above Eq.13 shows the variation of mass flow ratio for an axisymmetric inlet model when the oblique shock wave angle is changed from its previous state.

Figure 10 shows the variation of mass flow rate with the oblique shock angle β calculated theoretically based on Eq. 13 and compared with the present CFD results. Since the model used in the present study is axisymmetric, the theoretical variation of mass flow rate for different Mach numbers is presented. The semi-cone angle of the center body is 16 degrees, and it generates a shock angle of 46.73 degrees for a 2D planar intake at a Mach number of 2.0 and is
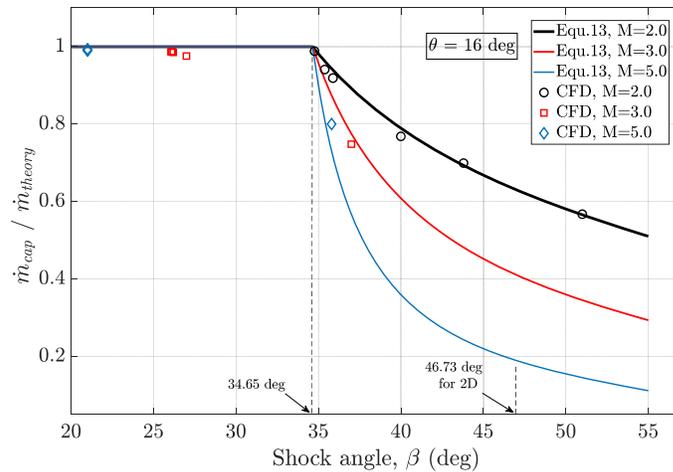
Fig. 8. Theoretical and CFD calculation of mass flow variation with the shock angle.

represented for reference purposes only. The solid line indicates the theoretical calculation whereas the discrete points denote the present CFD results. The x-axis is showing the oblique shock wave angle in the vicinity of the cowl lip and the y-axis indicates the ratio of captured mass flow to the theoretical mass flow rate. The present intake model is designed for a freestream Mach number of 2.0 and at this condition, the critical oblique shock wave angle is 34.6 degrees as indicated. If the oblique shock angle increases above this value, the mass flow rate through the inlet system is reduced concerning the inlet Mach number. The black thick line represents the theoretical calculation of mass flow rate with the oblique shock angle for M=2.0 while the black circles denote the corresponding value obtained in the CFD simulation. It is noted that at lower values of β, the deviation from the theoretical value is slightly larger compared to the larger values of β. This deviation is due to the formation of a second oblique shock on the compression ramp from the flow separation point. The actual theoretical model is not considering this fact, and in future studies, this variation with a correction factor has to be studied. The red line and red square points indicate the results at M=3 and the blue color line and blue diamond points indicate the results at M=5. The oblique shock wave angle in supercritical condition for M=3.0 is 26.1 degrees and this value is fairly constant at higher values of area ratio. The corresponding value of β is 21 degrees for M=5.0. The CFD results are in good agreement with the computation when the inlet is in subcritical operation, or at larger β values. The shock structure is having some curved bow shock wave when it is in critical or low subcritical operating modes. It is observed that the values of theoretical calculation and the obtained CFD results are in good agreement and one can predict the reduction in mass flow rate from the design condition by using this analysis.

3.3 Effect of Mach number and area ratio on performance parameters

For an inlet operating at a constant altitude, the total pressure and the static pressure are maintained

constant. If the engine accelerates at this condition, it is equivalent to increasing the dynamic pressure and hence the total pressure. Therefore, it is necessary to understand how much of this total pressure can be recovered in the engine. The performance parameters that are assessed numerically in this study are total pressure recovery (TPR), mass flow ratio (ξ). TPR is defined as the ratio of the total pressure at the intake exit face to the free stream total pressure. The intake exit total pressure is calculated by the area-weighted averaging of the total pressure monitored at the section before the exit plug.

$$TPR = \frac{P_{0,e}}{P_{0,\infty}} \tag{14}$$

Mass flow ratio is defined as the ratio of captured mass flow rate to the maximum possible theoretical flow rate that the intake can capture.

$$\xi = \frac{\dot{m}_{cap}}{\dot{m}_\infty} \tag{15}$$

The variation of the mass flow ratio ξ with the throat area ratio ψ for different Mach numbers is shown in Fig. 11. The abscissa is indicating the throat area ratio, and the left ordinate indicates the ratio of the mass flow rate through the inlet to the maximum possible mass flow rate at each Mach number and the right ordinate indicates the corresponding oblique shock angle. The flow rate through the inlet at supercritical conditions is the same as the captured mass flow rate and the maximum free stream flow rate is the same as the theoretical mass flow rate. It is noted that as the throat area ratio is reduced, the mass flow reduces after a particular area ratio. The region where the mass flow rate is constant is considered to be the supercritical operating mode and when the mass flow decreases, the inlet system changes to its subcritical operating mode. When ψ=1.16 the inlet is in the supercritical operating mode for all the Mach numbers and it can be identified from the earlier shock structures. Consider the case of M=2.0, where the value of ψ is decreased, it changes from supercritical to the subcritical mode by reducing the mass flow rate. This reduction in
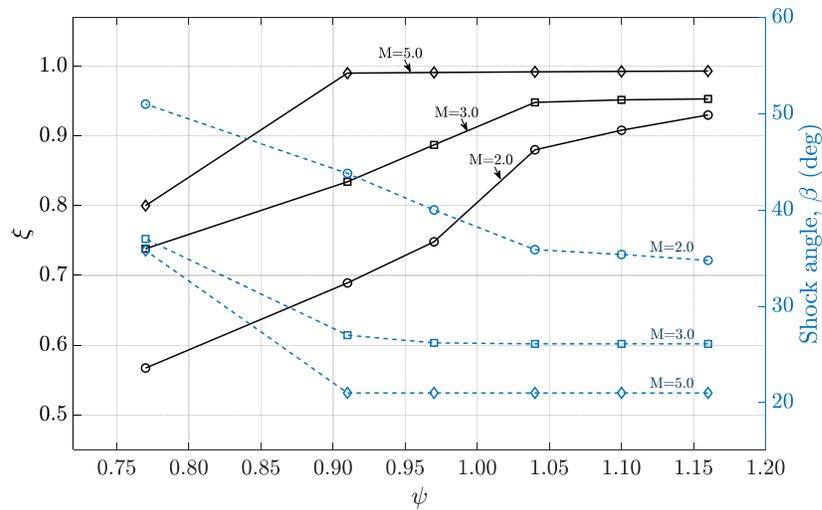
Fig. 9. Variation of the mass flow ratio and oblique shock angle with the throat area ratio for different Mach numbers.
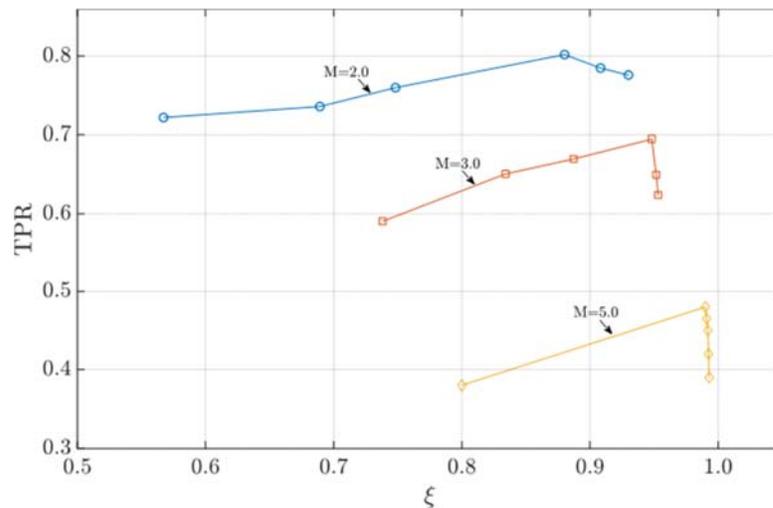

Fig. 10. Inlet performance curve showing the variation of TPR with the mass flow ratio at different Mach numbers.

mass flow rate is achieved by changing the oblique shock angle as shown in Fig. 10. The variation of the OSW angle at M=2.0 is also plotted in Fig. 11. It can be observed that as the area ratio is decreased, the OSW angle increases and it reduces the mass flow rate through the intake by increasing the spillage flow. Lower the area ratio, maximum is the spillage. At M=3.0, the mass flow rate remains constant up to an area ratio of 1.04, and the mass flow rate starts to reduce from this point. The variation in OSW angle is minimal until an area ratio of 0.97 and a further reduction in area ratio makes the inlet operate at subcritical conditions. Similarly, for M=5.0, the least value of ψ=0.77 turns the inlet into the subcritical operating condition. The backpressure required to change the shock angle is very large so that the inlet operates at supercritical conditions at large Mach numbers. As the Mach number is increased, the OSW angle at supercritical operating conditions also decreased.

Another performance parameter for an inlet is the total pressure recovery (TPR). The hypersonic propulsion system is designed to operate at different cruise speeds and hence it is equivalent to changing the stagnation pressure at each speed. Therefore, the stagnation pressure recovery has to be considered in detail for the performance analysis. Figure 12 shows the variation of TPR with ψ for different Mach numbers. The y-axis is normalized with the inlet stagnation pressure at each freestream Mach numbers. The stagnation pressure is measured at the end of the inlet region before the combustion chamber begins. In the present configuration, the measurements were taken at the region before the beginning of the downstream plug. It is noted that the TPR initially increases to a maximum value and then decreases when we reduce the throat area ratio. The larger value of TPR is obtained at a lower Mach number of M=2.0 and it reduces as the Mach number is increased to M=3 and 5. The maximum value for
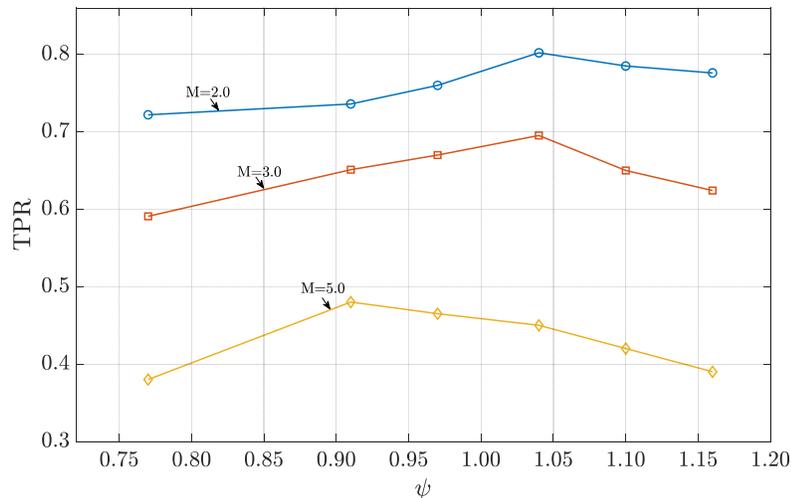
Fig. 11. Variation of total pressure recovery with the throat area ratio for different Mach numbers.

TPR is obtained at different ψ values for different Mach numbers. The case of M=2.0 has the maximum pressure recovery, while the highest mass flow rate is attained at a free-stream Mach number of 5.0, but the pressure recovery decreases due to changes in the shock wave structure that forms in the inlet.

Also, it will decrease the shock angle that forms at the nose of the spike and reduce the mass spillage. The losses associated with larger Mach numbers are higher and hence the overall TPR is reduced at larger Mach numbers. Thus, the analysis of TPR can be helpful for the optimum design of a hypersonic propulsion system with the best performance.

Finally, in this section, the intake performance curve is represented in Fig. 13 for all free stream Mach numbers. According to this figure when the free stream Mach number increases the intake TPR decreases but the mass flow ratio increases. This inlet performance curve along with the shock structure variation and oblique shock angle variation can give an enhanced insight into the design of a hypersonic inlet system with an optimum operating condition. The present study was an attempt to demonstrate the relationship between the OSW angle variation and the analysis of performance parameters by considering air as an ideal gas. But future work on exploring the inlet operation by considering the real gas effect and the complex geometries can provide a large overview of the supersonic inlet performance.

4.   CONCLUSIONS

A simple two-dimensional axisymmetric hypersonic mixed compression inlet is considered to understand the fluid flow observed in the inlet due to the exit area variation and freestream Mach number variation by numerical means. The exit area ratio variation is simulated by placing a wedge-plug at different axial locations at the exit of the inlet model. The flow field is achieved computationally by solving the Reynolds Navier-Stokes (RANS) equations with a kω-SST turbulence model. The computational results were validated with the wind tunnel data of an intake from

the earlier reference work, designed to operate at a free-stream Mach number of 2.0. The results for this specific intake were in good agreement between the numerical and experimental results. Initially, the shock structure variations for different area ratios at different Mach numbers were analyzed. The result shows that as the area ratio is increased, there can be a possibility of a reduction in mass flow rate by changing the oblique shock wave angle. Hence the relationship between the oblique shock angle and the mass flow rate at different area ratios and Mach number is calculated theoretically. The computational results were compared with the theoretical values and it is found that the design free steam Mach number condition was in good agreement with the theoretical value. This method quantifies the reduction in mass flow rate through the throttling effect by analyzing the flow field structure in terms of the oblique shock angle. Later the performance parameters of the inlet are analyzed utilizing mass flow ratio and the total pressure recovery. The mass flow rate remains constant until the critical operation point and reduces as the ψ value is increased for each Mach number. It is also indicated that the maximum mass flow attained increases with an increase in Mach number. The total pressure recovery was reduced when the free stream Mach number was increased, which was caused by the strengthening of the shocks. The losses associated with larger Mach numbers are higher and hence the overall TPR is reduced at larger Mach numbers.

REFERENCES

Abedi, M., R. Askari and M. R. Soltani (2020). Numerical   simulation   of   inlet   buzz.

Aerospace Science and Technology 97, 105547.

Chang, J., W. Bao, Y. Fan and D. Yu (2009). Performance optimization of hypersonic inlets with pulse periodic energy addition. *Proceedings of the Institution of Mechanical Engineers, Part G: Journal of Aerospace Engineering* 223(6), 691–699.

Chen, X., C. Zhou, Y. Zheng and Y. Ju (2005a). Influence of cowl leading edge on inlet performance of ramjet assisted-range projectiles. *41st AIAA/ASME/SAE/ASEE Joint Propulsion Conference and Exhibit*, 3642.

Chen, X., Y. Zheng, C. Zhou and Y. Ju (2005b). Numerical simulation on ramjet inlet with different cowl leading edge. *35th AIAA Fluid Dynamics Conference and Exhibit*, 5288.

Clemens, N. T. and V. Narayanaswamy (2014). Low-Frequency Unsteadiness of Shock Wave/Turbulent Boundary Layer Interactions. *Annual Review of Fluid Mechanics* 46(September), 469–492.

Curran, E. T. and S. N. B. Murthy (2001). Scramjet Propulsion. In S. N. B. Murthy and E. T. Curran (Eds.), *AIAA*. American Institute of Aeronautics and Astronautics.

Das, S. and J. K. Prasad (2009). Cowl deflection angle in a supersonic air intake. *Defence Science Journal* 59(2), 99–105.

Das, S. and J. K. Prasad (2010). Starting characteristics of a rectangular supersonic air-intake with cowl deflection. *Aeronautical Journal* 114(1153), 177–189.

Fan, J. (2011). Optimal speed of hypersonic cruise flight. *Theoretical and Applied Mechanics Letters* 1(1), 012004.

Gokhale, S. S. and V. R. Kumar (2001). Numerical computations of supersonic inlet flow. *International Journal for Numerical Methods in Fluids* 36(5), 597–617.

James, K. J., A. Suryan and H. D. Kim (2021). Buzz characteristics and separation bubble dynamics in supersonic intake. *Aerospace Science and Technology* 115, 106795.

Lee, J. and S. H. Kang (2019). Numerical study on the start and unstart phenomena in a scramjet inlet-isolator model. *PLOS ONE*, 14(11), e0224994.

Li, N., J. T. Chang, K. J. Xu, D. R. Yu, W. Bao and Y. P. Song (2017). Prediction dynamic model of shock train with complex background waves. *Physics of Fluids* 29(11), 116103.

Li, N., J. T. Chang, K. J. Xu, D. R. Yu, W. Bao and Y. P. Song (2018). Oscillation of the shock train in an isolator with incident shocks. *Physics of Fluids* 30(11), 116102.

Liang, J. H., X.-Q. Fan, Y. Wang and W. D. Liu (2008). Performance enhancement of three-dimensional hypersonic inlet with sidewall compression. *Proceedings of the Institution of Mechanical Engineers, Part G: Journal of Aerospace Engineering* 222(8), 1211–1219.

Marguart, E. J. (1991). Predictions and measurements of internal and external flow fields of a generic hypersonic inlet. *9th Applied Aerodynamics Conference*, 3320.

Menter, F. (1993). Zonal Two Equation k-w Turbulence Models For Aerodynamic Flows. *23rd Fluid Dynamics, Plasmadynamics, and Lasers Conference*, 2906.

Menter, F. R. (1994). Two-equation eddy-viscosity turbulence models for engineering applications. *AIAA Journal* 32(8), 1598–1605.

Nair, M. T., N. Kumar and S. K. Saxena (2005). Computational analysis of inlet aerodynamics for a hypersonic research vehicle. *Journal of Propulsion and Power* 21(2), 286–291.

Raj, N. O. P. and K. Venkatasubbaiah (2012). A new approach for the design of hypersonic scramjet inlets. *Physics of Fluids* 24(8), 086103.

Ram, P., T. Kim and H. Kim (2020). Numerical study on shock train characteristics in divergent channels. *Journal of Applied Fluid Mechanics* 13(4), 1735–3645.

Roy, C. J. and F. G. Blottner (2006). Review and assessment of turbulence models for hypersonic flows. *Progress in Aerospace Sciences* 42(7–8), 469–530.

Soltani, M. R., J. S. Younsi, M. Farahani and A. Masoud (2013). Numerical simulation and parametric study of a supersonic intake. *Proceedings of the Institution of Mechanical Engineers, Part G: Journal of Aerospace Engineering* 227(3), 467–479.

Van Wie, D. M., F. T. Kwok and R. F. Walsh (1996). Starting characteristics of supersonic inlets. *32nd Joint Propulsion Conference and Exhibit*, 2914.

Wang, W. and R. Guo (2013). Numerical study of unsteady starting characteristics of a hypersonic inlet. *Chinese Journal of Aeronautics* 26(3), 563–571.

Wang, Z., J. Chang, W. Hou and D. Yu (2020). Low-frequency unsteadiness of shock-wave/boundary-layer interaction in an isolator with background waves. *Physics of Fluids* 32(5), 056105.

Weir, L., D. R. Reddy and G. Rupp (1989). Mach 5 inlet CFD and experimental results. *25th Joint Propulsion Conference*, 2355.

Xiang, G. X., C. Wang, H. H. Teng and Z. L. Jiang (2016). Investigations of Three-Dimensional Shock/Shock Interactions over Symmetrical Intersecting Wedges. *AIAA Journal* 54(5), 1472–1481.

Xiang, G. X., X. Gao, W. J. Tang, X. Z. Jie and X. Huang (2020a). Numerical study on transition structures of oblique detonations with expansion wave from finite-length cowl. *Physics of Fluids* 32(5), 056108.

Xiang, G., X. Gao, X. Jie, X. Li, H. Li and X. Chen (2020b). Flowfield characteristics in sidewall compression inlets. *Acta Mechanica Sinica*, 36(3), 678–685.

Xiang, G., Y. Zhang, X. Gao, H. Li and X. Huang (2021). Oblique detonation waves induced by two symmetrical wedges in hydrogen-air mixtures. *Fuel* 295, 120615.

Zha, G. C., D. Smith, M. Schwabacher, K. Rasheed, A. Gelsey, D. Knight and M. Haas (1997). High-performance supersonic missile inlet design using automated optimization. *Journal of Aircraft* 34(6), 697–705.